Revision-1

New high pressure phases in MOOH (M=Al, Ga, In)

ASHOK K. VERMA[1], P. MODAK[1] and LARS STIXRUDE[2]

[1]High Pressure and Synchrotron Radiation Physics Division,
Bhabha Atomic Research Centre, Trombay, Mumbai – 400085, India
[2]Department of Earth Sciences, University College London, Gower Street, London,
WC1E 6BT, United Kingdom

Abstract

A unique phase, belonging to an orthorhombic crystal system (*Pbca*, Z = 8), is proposed in AlOOH using crystal structure searches based on an evolutionary genetic algorithm method combined with density functional theory. This phase features a nonlinear asymmetric doubly-covalent hydrogen-bond and metal cations that are six-fold oxygen coordinated. Unlike the earlier proposed monoclinic phase, the stability region of *Pbca* (166-189 GPa) lies well below the pressure of decomposition to Al_2O_3+ice X (287 GPa). In GaOOH the *Pbca*-type phase is not energetically favourable at any pressure. In the course of evaluating the breakdown of GaOOH to its constituent oxides, we have found a new phase of Ga_2O_3 (U_2S_3-type). In InOOH, *Pbca* is energetically favourable over a narrow pressure interval (12-17 GPa). Also in InOOH, we find a new tetragonal structure ($P\bar{4}2_1m$, Z = 4) stable above 51 GPa. This phase has nonlinear asymmetric hydrogen-bonds and metal cations that are seven-fold oxygen coordinated. Phonon calculations confirm the vibrational stability of the new phases and show that the high pressure polymorphs of AlOOH are likely to be important carriers of water into the deep lower mantles of Earth and rocky super-Earths.

INTRODUCTION

Hydrogen is an important component of the solid Earth, where even in small concentrations it can have a major effect on physical properties including the melting temperature, rheology, and seismic wave velocities (Williams and Hemley 2001). The hydrogen contained in minerals is an important part of the long term water cycle: there may be more hydrogen bound in the mantle than there is in the surface ocean. Hydrogen bound in minerals is likely to be an important part of the water cycle on rocky exoplanets as well, including super-Earths (Tikoo and Elkins-Tanton, 2017).

Despite its importance, our knowledge of where hydrogen is stored throughout most of the pressure range of planetary mantles is still very limited, particularly at conditions of the Earth's lower mantle (24-136GPa; 1000-4000 K) and beyond: the mantle of a 2 Earth-mass super-Earth may extend to 270 GPa (Stixrude 2014). A key question is whether hydrous minerals: minerals in which hydrogen is present in stoichiometric quantities, rather than merely as defects, can be stable in the deep interiors of rocky planets.

The AlOOH component appears to be essential for stabilizing hydrous phases at lower mantle conditions. The stability field of phase H is much wider in the MgO-SiO_2-Al_2O_3-H_2O (MASH) system than in the MSH system and encompasses the ambient lower mantle geotherm up to the pressure of the core-mantle boundary (Nishi et al., 2014; Walter et al., 2015). In contrast, the stability fields of hydrous phases in the MgO-SiO_2-H_2O system found so far are limited and none are stable at conditions of the ambient lower mantle (Nishi et al., 2014; Walter et al., 2015). The greater stability of phase H in aluminous systems has a structural origin. Phase H has composition $MgSi(OOH)_2$ and a structure commensurate with that of the δ-phase of AlOOH. In aluminous systems, phase H is found to consist of a near complete solid solution between these two end-

members. The alumina content of phase H in a typical mantle bulk composition is estimated to be 40 % (Walter et al., 2015).The δ-AlOOH phase is also commensurate with the post-stishovite $CaCl_2$-type phase of silica with which it may form a solid solution (Panero and Stixrude, 2004) that could be an important hydrous phase in more silica-rich compositions such as subducted oceanic crust. Studies of the AlOOH solid solutions are limited to the pressure range of Earth's mantle and their stability at the high pressure-temperature conditions expected in deep super-Earth mantles is unknown.

Because of its crucial role in stabilizing hydrous phases in the lower mantle and the structural relationship with the H phase and $CaCl_2$-type silica, end-member AlOOH serves as an ideal model system for understanding the nature of hydrous phases that may occur in Earth's mantle and super-Earth mantles. Experimentally, the only known high pressure phase is δ-AlOOH ($P2_1nm$, Z = 2), first synthesized at 21 GPa and 1000 ^{0}C (Suzuki et al. 2000), and subsequently observed up to 120 GPa (Sano et al. 2008). The phase has a wide temperature stability field up to conditions comparable to those present in Earth's mantle (2000 K at 70 GPa). The δ-phase also serves as a paradigm for the fundamental changes to hydrogen bonding that occur at high pressure: on compression the hydrogen bond symmetrises, raising the symmetry to *Pnnm* and producing large anomalies in elastic and vibrational properties (Tunega et al. 2011; Cedillo et al. 2016)). The stability field, symmetrisation, and physical properties of this phase have been the subject of numerous studies (Tsuchiya et al. 2002; Tsuchiya et al. 2004; Panero and Stixrude 2004; Li et al. 2006; Tsuchiya et al. 2008a; Furukawa et al. 2008; Kuribayashi et al. 2014; Duan et al. 2018).

Recently two groups examined the structure of AlOOH at much higher pressure using first-principles density functional calculations (Tsuchiya and Tsuchiya 2011;

Zhong et al. 2016). These studies found two mechanically stable high pressure structures: pyrite-type ($Pa\bar{3}$, Z = 4) at 170 GPa (Tsuchiya and Tsuchiya 2011), and a monoclinic structure ($P2_1/c$, Z = 4) at 340 GPa (Zhong et al. 2016). This latter phase however is not energetically favourable at any pressure as AlOOH decomposes to its constituent oxides: $CaIrO_3$-type Al_2O_3 ($Cmcm$, Z = 4) (Umemoto and Wentzcovitch 2008) and ice X ($Pn\bar{3}m$, Z = 2) at ~300 GPa (Caracas 2008).

As the predicted new phases are only stable at pressures much higher than those accessible to most experiments, we gain additional insight into the behaviour of AlOOH by examining homologues (Neuhaus 1964). Indeed recent studies have found that AlOOH, GaOOH and InOOH exhibit the same sequence of structural transitions at elevated pressures and transition pressures of the GaOOH and InOOH were found to be lower than those of the AlOOH(Tsuchiya and Tsuchiya 2011; Zhong et al. 2016). Calculated pressures for the decomposition also follow the homologous rule (Zhong et al. 2016).

Here we perform extensive first-principles crystal structure searches in AlOOH, GaOOH, and InOOH over a wide pressure range, revealing new phases. Our results allow us to examine the sequence of phase transitions previously proposed in these systems, and to further test the idea that GaOOH and InOOH may serve as homologues for the behaviour of AlOOH.

METHODOLOGY

Crystal structure searches are performed at 0 (1, 2, 4, 8 formula units), 50 (1, 2, 4 formula units), 100 (1, 2, 4 formula units), 150 (1, 2, 4, 6, 8 formula units), 250 (1, 2, 4, 8 formula units) and 300 GPa (1, 2, 4 formula units) for AlOOH using the USPEX code in combination with VASP (Oganov et al. 2006; Lyakhov et al. 2013; Oganov et al. 2011;

Kresse and Hafner 1994; Blöchl 1994; Kresse and Furthmuller 1996; Kresse and Joubert 1999). Additional structural searches are performed for GaOOH and InOOH at 175 GPa (1, 2, 4, formula units) and 50 GPa (1, 2, 4 formula units), respectively. The first generation in crystal structure searches is prepared randomly at fixed density, and structures are subsequently optimized at the desired pressure. The initial population is taken to be 10-90 depending upon the total number of atoms in the simulation cell. Normally the crystal structure searches are run up to 10-20 generations. Previously this methodology has been successfully used to predict and solve the crystal structures of a large number of systems under diverse pressure conditions (e.g., Oganov and Ono 2004; Verma et al. 2017; Modak and Verma 2017; Patel et al. 2017).

In crystal structure searches the plane-wave basis set is constructed using a 500 eV energy cutoff and the Brillouin zone is sampled using Monkhorst-Pack method (Monkhorst and Pack 1976) with a grid spacing of $2\pi \times 0.06$ Å^{-1}. For re-optimization of the lowest energy structures, the plane-wave basis set energy cutoff is increased to 600 eV and reciprocal space integration is done with a finer grid spacing of $2\pi \times 0.03$ Å^{-1}. Atomic positions are relaxed until the forces become smaller than 2.0 meVÅ^{-1}. The chosen computational parameters insure the convergence of total energies better than 1.0 meV per atom. The crystal structure searches are performed using GGA (Perdew et al. 1996), while we have used both GGA and LDA (Perdew and Zunger 1982) to further investigate the physical properties of the phases that we have found. All electron frozen-core projector-augmented wave (PAW) potentials are used with Al ($3s^2$, $3p^1$), Ga ($3d^{10}$, $4s^2$, $4p^1$), In ($4d^{10}$, $5s^2$, $5p^1$), O ($2s^2$, $2p^4$) and H ($1s^1$) valence configurations. These potentials have cutoff radii of 1.9 (Al), 2.3 (Ga), 2.5 (In), 1.52 (O) and 1.1 (H) atomic units (a. u.). Some of the highest pressure results of AlOOH and GaOOH are verified with still harder PAW potentials (1200 eV cutoff). Phonon calculations are performed using

the supercell method as implemented in the PHON code (Alfe 2009). A 1 × 2 × 2 supercell is used for *Pbca*-type AlOOH (at 180 GPa) and a 2 × 2 × 2 supercell is used for $P\bar{4}2_1m$-type InOOH (at 60 GPa). Additional phonons are calculated for *Pnnm* and $Pa\bar{3}$ phases of AlOOH using 2 × 2 × 4 and 2 × 2 × 2 supercells, respectively.

We also use phonon calculations to compute the influence of temperature on the phase transition boundaries. The Helmholtz free energy

$$F(V,T) = E_{static}(V) + E_0(V) + F_{TH}(V,T) \quad (1)$$

where E_{static} is the total energy from our static calculations, E_0 is the zero point energy and $F_{TH}(V,T)$ is the thermal contribution arising from phonon excitations. Phase boundaries are defined by equality of the Gibbs free energy, G, of the two phases and the Legendre transform

$$G = F + PV \quad (2)$$

where the pressure $P = -(\partial F/\partial V)_T$.

RESULTS

(a) AlOOH

Crystal structure searches yield all known crystal structures for AlOOH. Enthalpy-pressure relations for the most stable structures are plotted in Fig. 1. GGA calculations fail to reproduce the diaspore phase (*Pbnm*, Z = 4) as the ground state structure, while LDA correctly recovers the ground state, in agreement with previous works (e.g., Cedillo et al. 2016; Tsuchiya and Tsuchiya 2011; Friedrich et al. 2007). Although LDA correctly predicts the ground state structure, it fails to predict the subsequent phase transitions correctly. Also in LDA calculations the δ-phase ($P2_1nm$, Z = 2) always relaxes to the hydrogen-bond symmetrized *Pnnm* structure at positive pressures. GGA predicts the diaspore to δ-AlOOH phase transition correctly (Table I), so at elevated pressures GGA results are more accurate than LDA. Interestingly the earlier proposed boehmite

structure ($Cmc2_1$, Z = 4) (Tunega et al. 2011) has slightly higher enthalpy than a trigonal structure ($R\bar{3}m$, Z = 3) in LDA calculations; this trigonal structure is also mechanically stable in GGA, although it is never more stable than $Cmc2_1$. Note that the enthalpy of the experimentally proposed structure (*Cmcm*, Z = 4) lies above the energy-range of plots. Notably the relaxed *Cmcm* structure has symmetrised hydrogen-bonds in GGA and LDA. The edge-sharing AlO_6 octahedra of $R\bar{3}m$ are arranged in (001) plane and these layers are joined together by hydrogen-bonds along *c* direction.

At 166 (159) GPa, GGA (LDA) calculations show the transformation of the δ-phase (*Pnnm*) to a new orthorhombic phase (*Pbca*, Z = 8). This is the first proposed structure in this family of compounds which has eight-formula units in the primitive cell. The *Pbca* phase is stable from 166 GPa to 189 GPa, where it transforms to the pyrite structure. Thus the stability field of *Pbca* lies well below the pressure of decomposition to oxides, which has been found in previous studies to be 295 GPa (Zhong et al. 2016) and 300GPa (Tsuchiya and Tsuchiya 2011). Similar to the *Pnnm* and $Pa\bar{3}$ phases, the *Pbca* phase has six-fold oxygen coordinated aluminium cations (Fig. 2). The linear symmetric hydrogen-bond configuration of the *Pnnm* phase changes to a nonlinear asymmetric configuration in *Pbca*. At 170 GPa, GGA (LDA) ∠OHO is 166º (169º) and the hydrogen-bond lengths are 1.08 (1.09) and 1.15 (1.15) Å. GGA (LDA) Al–O bond-lengths are spread over 1.73 (1.69)– 1.74 (1.72) Å. Detailed structural information is presented in Table II. For comparison, at 170 GPa, in the $Pa\bar{3}$ phase the hydrogen-bond length is 1.11 Å and the Al–O bond-lengths are 1.73 Å in GGA. Both O–H bond lengths in the *Pbca* phase decrease with pressure, like doubly-covalent symmetric hydrogen bonds (Fig. 3) (Sikka and Sharma 2008). At 170 GPa, the GGA band-gap, 10.84 eV, of this phase is slightly bigger than the $Pa\bar{3}$ phase, 10.73 eV.

We may compare the new *Pbca* structure to that of seifertite-type AlOOH (*Pbcn*, *Z* = 4), which is not energetically favourable, but is mechanically stable. This is an intriguing comparison because of the parallels between the phase transformations in AlOOH and SiO_2 *via* $Si^{4+} \rightarrow Al^{3+} + H^{+}$ substitution (e.g., Panero and Stixrude 2004; Tsuchiya and Tsuchiya 2011; Karki et al. 1997; Martonak et al. 2006). The sequence of AlOOH polymorphs: δ-phase, *Pbca*, and pyrite is very similar to that seen in SiO_2: $CaCl_2$-type structure (identical to the anhydrous sub-lattice of the δ-phase), seifertite, and pyrite. Thus the *Pbca* phase in AlOOH takes the place of the seifertite phase in SiO_2. The enthalpy of seifertite-type AlOOH is nearly parallel to that of the *Pnnm* phase, and, like the *Pnnm* phase, has symmetric hydrogen bonds. This marks a crucial difference with the *Pbca* phase, which has asymmetric hydrogen bonding.

Also, unlike the seifertite structure in which cations form zigzag chains of edge-shared octahedra, the *Pbca* phase has only pairs of edge-shared octahedra. In the *Pbca* phase, anions form a chain-like pattern in the (010) plane (Fig. 2). Thus *Pbca* differs from earlier proposed structures of SiO_2 which consist of chains of edge-shared SiO_6 octahedra with oxygen atoms arranged in a hexagonal-close-pack array (Teter et al. 1998).

Both LDA and GGA cell parameters and pressure-volume relations agree fairly well with experiment (Figs. 4 & 5). The equation of state of *Pbca* phase lies between that of *Pnnm* and $Pa\bar{3}$ phases. Upon the *Pnnm* to *Pbca* phase transformation there is a 1.58% (1.66) volume drop in GGA (LDA) calculations. The *Pbca* to $Pa\bar{3}$ phase transition leads to a volume drop of ~0.70% (0.66). Dynamical stability is assessed by calculating the phonon dispersion relations and their density of states: the absence of imaginary phonon frequencies establishes the dynamic stability of the *Pbca*-type phase (Fig. 6).

We combine static calculations with phonon calculations to determine the AlOOH phase diagram (Fig.7). Each of the high pressure phase transitions (δ to *Pbca*, *Pbca* to pyrite, and pyrite to oxides) shows a slightly negative Clapeyron slope, with the pressure of the transition decreasing slightly with increasing temperature in the range 0-4000 K.

We use our results to estimate the high temperature stability limit of AlOOH to pressures beyond those of the highest pressure experiments (80 GPa, Sano et al., 2008). The curve must join the triple point:

$$\text{AlOOH (pyrite)} = Al_2O_3\ (CaIrO_3) + \text{Ice SI} = Al_2O_3\ (CaIrO_3) + \text{Ice X} \qquad (3)$$

Because the $CaIrO_3$ phase of Al_2O_3 appears twice in Eq. (3), the triple point is the intersection of the AlOOH (pyrite) = Al_2O_3 ($CaIrO_3$) + Ice X curve and the Ice X = Ice SI curve, where Ice SI indicates the superionic form of ice. The Ice X = Ice SI curve (Kimura et al., 2014) intersects the AlOOH (pyrite) = Al_2O_3 ($CaIrO_3$) + Ice X curve at 1790 K and 290 GPa. We have fit a smooth curve through our estimated triple point and the experimental data of Sano et al. (2008) yielding the following equation for thermal stability limit of AlOOH, valid from 17 GPa to the triple point:

$$T = T_0 \left(1 + \frac{\Delta P}{a}\right)^b \exp\left(-\frac{\Delta P}{c}\right) \qquad (4)$$

with $T_0 = 1350$ K, $\Delta P = P - 17$GPa, a = 82 GPa, b = 1.95, c = 106 GPa, and we have used the form suggested by Kechin et al. (2001). In drawing this curve we have assumed, following the analysis of Millot et al. (2018) that the measurements of Kimura et al.

(2014) detect the Ice X to superionic ice transition. We have also assumed that AlOOH breaks down to Al_2O_3 + superionic ice at pressure greater than 80 GPa, where the AlOOH dehydration curve of Sano et al. (2008) intersects the superionic ice to H_2O fluid transition of Millot et al. (2018). Our analysis assumes that AlOOH does not transform to a superionic form at high temperature, which our results cannot rule out, and for which there is currently no evidence in the literature. Zhong et al. (2016) speculated that superionic AlOOH may be stabilized at high temperature, in which case the effect on the phase diagram would likely be to expand the AlOOH stability field to higher temperature.

(b) GaOOH

The high-pressure structural behaviour of GaOOH differs significantly from that of AlOOH, violating the homologous rule. The orthorhombic *Pbca*-type structure never becomes energetically favourable in GaOOH (Fig.8). The monoclinic $P2_1/c$-type phase also never becomes energetically favourable at elevated pressures, unlike the results of an earlier study (Zhong et al. 2016). Instead, we find that GaOOH decomposes directly from the pyrite-type structure to its constituent oxides: Ga_2O_3 (U_2S_3-type, *Pnma*, Z = 4) and ice ($Pn\bar{3}m$, Z = 2) at 240GPa (GGA).

To better understand the discrepancy between our results and those of (Zhong et al. 2016), we focus on the pressure of the (metastable) $Pa\bar{3}$ to $P2_1/c$ phase transition and the role of the Ga PAW potential. Whereas we find the transition to occur at 243 GPa, Ref. (Zhong et al. 2016) finds the transition at a much lower pressure (170.5 GPa). We attribute this difference to the fact that we have used a harder Ga PAW potential, with R_{cut}=2.3 a.u. as compared with (Zhong et al. 2016) who used a Ga PAW potential with R_{cut}=2.6 a.u. To test this explanation, we have repeated our calculations with the softer Ga PAW potential. Indeed, we find the $Pa\bar{3}$ to $P2_1/c$ transition pressure to occur

at 171.6 GPa using the softer potential, in perfect agreement with the result of (Zhong et al. 2016). Moreover, with the softer PAW potential, we also find, as did (Zhong et al. 2016), that GaOOH never breaks down to constituent oxides, with the enthalpy curve of GaOOH becoming ever more favourable with respect to Ga_2O_3+ice with increasing pressure. We have further checked our results against an even harder set of PAW potentials with: R_{cut} = 1.9 a.u. (Ga), 1.1 (O), and 0.8 a.u. (H), and find the transition again to occur at 243 GPa.

Another difference from the earlier study (Zhong et al. 2016) is that we find a new stable structure of Ga_2O_3 (Fig. 9). Whereas the previous study assumed the $CaIrO_3$-type structure for Ga_2O_3, we find, as the result of extensive structural optimizations, that the U_2S_3-type structure is more stable. Thus, we predict a new phase transformation in Ga_2O_3 at 200 GPa from $CaIrO_3$- to U_2S_3-type structure. The U_2S_3-type structure was proposed to stabilize in Al_2O_3 at 370 GPa in earlier work (Umemoto and Wentzcovitch 2008).

(c) InOOH

The sequence of high pressure phase transformations in InOOH differs from that in AlOOH and GaOOH (Fig. 10). As in the case of AlOOH, GGA and LDA calculations show different behaviour in low-pressure region, 0-25 GPa. At zero pressure LDA produces the correct ground state phase (*Pnnm*) whereas GGA wrongly predicts diaspore as the ground state. GGA results are in accordance with earlier calculations (Tsuchiya et al. 2008b).

In GGA calculations, the orthorhombic *Pbca*-type phase becomes energetically favourable over a narrow pressure interval (12.4 – 17.3 GPa), whereas in LDA calculations this phase never stabilizes. The difference between GGA and LDA

predictions for this phase transition is consistent with a widely recognized trend: LDA and GGA usually underestimate and overestimate phase transition pressures, respectively (e.g., Modak and Verma 2011; Yusa et al. 2008). Further increase in pressure stabilizes a new tetragonal structure ($P\bar{4}2_1m$, Z = 4) at ~ 51 (47) GPa in GGA (LDA). This is the first proposed tetragonal structure in this entire family of MOOH compounds. Note that the monoclinic $P2_1/c$-type structure never becomes energetically superior to the tetragonal structure upto 100 GPa. The tetragonal phase has asymmetric nonlinear hydrogen-bonds (1.01, 1.49 Å and ∠OHO = 178.3°) and the metal cation is seven-fold oxygen coordinated (Fig. 2) with In-O bond-lengths varies from 2.05 – 2.23 Å at 60 GPa in GGA. In this phase edge- and face-shared InO_7polyhedra form a chain-like pattern (Fig. 2). Note that the monoclinic $P2_1/c$ structure also has seven-fold oxygen coordinated cations (edge-share) and nonlinear asymmetric hydrogen-bonds. There is a 3.2 (3.9) % volume drop upon the transition to the tetragonal phase in GGA (LDA) calculations (Fig. 11).The GGA electronic band-gap of tetragonal phase, 3.05 eV, is slightly smaller than that of the$Pa\bar{3}$ phase, 3.28 eV, at 60 GPa. The vibrational stability of the tetragonal phase is confirmed by phonon calculations (Fig. 12). Our results are consistent with experiments: Ref. (Sano et al. 2008b) made measurements between 14 and 30 GPa, finding the pyrite structure to be stable over this range of pressure, as compared with our pyrite stability field: 17.3-50 GPa. As measurements were not conducted between0 and 14 GPa, it is possible that this experiment missed the *Pbca* phase, which we predict to be stable up to 17.3 GPa. We find that tetragonal InOOH decomposes into In_2O_3 (α-Gd_2S_3-type, *Pnma*, Z = 4) and ice X at ~78GPa in GGA. In earlier calculations monoclinic InOOH decomposes into In_2O_3 (α-Gd_2S_3-type, *Pnma*, Z = 4) and ice X at 77 GPa in GGA (Zhong et al. 2016).

DISCUSSION

Our predictions are amenable to experimental tests with current capabilities. For example, our predicted *Pbca* stability field in AlOOH (166-189 GPa) lies just beyond the range of the previous highest pressure study in this system (134 GPa) (Sano et al. 2008a), and well within the range previously explored in other low atomic number systems (e.g., Sakai et al. 2016). In the case of InOOH, our predicted *Pbca* stability field lies within the pressure regime of existing measurements, and we suggest that the previous experimental study may have skipped over the *Pbca* stability field and into that of the next higher pressure polymorph (pyrite-type). A more thorough examination in the pressure range 0-17 GPa is thus warranted in the InOOH system. Moreover, in InOOH, we predict another new phase ($P\bar{4}2_1m$) stabilized at modest pressures (51 GPa), well within current experimental capability.

Our results show the limitations of the homologous rule. The high-pressure sequence of phase transformations in AlOOH ($\delta \rightarrow Pbca \rightarrow Pa\bar{3} \rightarrow$ oxides), GaOOH ($\delta \rightarrow Pa\bar{3} \rightarrow$ oxides), and InOOH ($\delta \rightarrow Pbca \rightarrow Pa\bar{3} \rightarrow P\bar{4}2_1m \rightarrow$ oxides) are all different. As the homologous rule is rationalized in terms of ionic radius, we attribute the breakdown of homology to variations in the ionicity and bonding with increasing atomic number and pressure. Indeed, a previous study has shown that the Bader charges on the M cation decrease monotonically with increasing atomic number in the MOOH series (Zhong et al. 2016). Moreover, the band structure of GaOOH and InOOH (Zhong et al. 2016) both show significant hybridization between the O 2*p* states and *d*-states that are absent in AlOOH. In detail, while variations in ionicity and hybridization explain the breakdown of homology, they cannot account in any simple way for various trends in phase transformation sequences across the series, highlighting the importance of full electronic structure calculations of energetics as we have done: for example the

appearance of *Pbca* in the lightest and heaviest compounds (AlOOH and InOOH) and its absence in the intermediate compound (GaOOH).

Hydrogen bonding in the *Pbca* phase differs from that of many high pressure hydrous oxides and silicates in that the hydrogen bond is doubly-covalent (O-H-O), yet asymmetric. In many systems, an asymmetric O-H…O hydrogen bond is stable at low pressure, and as pressure increases, this hydrogen bond eventually becomes symmetric: O-H-O, with two equal O-H bond lengths and a linear geometry, as in the $P2_1nm$-$Pnnm$ transition of the δ-phase of AlOOH (Tsuchiya 2002), the Ice VII-Ice X transition in H_2O (Goncharov et al. 1996), and phase D (Tsuchiya et al.2005). The symmetric hydrogen bond also differs from the asymmetric hydrogen bond in the pressure dependence of the bond lengths: whereas in the typical asymmetric hydrogen bond the O-H bond expands and the H…O bond contracts on compression, in the symmetrically bonded case, both O-H bonds contract equally on compression. In contrast, the hydrogen bond in *Pbca* is asymmetric, yet both O-H bonds contract on compression. Moreover, the hydrogen bond in *Pbca* is non-linear.

The MOOH family highlights an important limitation of crystal structure searches. Because the size of configuration space grows exponentially with the size of the unit cell, in practice searches must place a limit on the maximum size of the unit cell to be considered. This limitation means that it is possible to miss energetically favourable crystal structures with unit cells that are larger than the practical maximum size. Whereas previous studies had considered unit cells up to Z= 4, we have found a new structure with Z= 8: the *Pbca* phase, which has a predicted GGA stability field in AlOOH, and InOOH, although not in GaOOH.

IMPLICATIONS

The phase diagram (Fig. 7) shows that the polymorphs of AlOOH are stable over a wide range of pressure-temperature conditions expected to occur in Earth and super-Earth mantles. AlOOH is therefore likely to be an important component of hydrous phases in super-Earths as it is in Earth's mantle where it forms the major lower mantle hydrous phase in solid solution with $MgSi(OOH)_2$.

Cold downwellings lie within the stability field of AlOOH down to the bottom of rocky planetary mantles with masses up to twice that of Earth. The high pressure polymorphs of AlOOH are therefore likely to be important carrier of water into deep telluric mantles. As downwellings warm to ambient mantle temperature, or descend to even greater depths as could occur in super-Earths more than twice as massive as Earth, AlOOH breaks down to a solid phase assemblage of Al_2O_3 and superionic ice. The high pressure polymorphs that we find therefore do not dehydrate in deep terrestrial mantles (P>80 GPa): no fluid phase is produced and water remains bound in solid phases.

Our results show the importance of understanding the solid solution between AlOOH and MgSi oxi-hydroxide components at deep lower mantle conditions (Nishi et al., 2014, Walter et al., 2015). In telluric planetary mantles, AlOOH is likely to contain significant amounts Mg and Si in solid solution in the form of the $MgSi(OOH)_2$ component. Experimental results to date show that end-member $MgSi(OOH)_2$ is cation disordered and has the same space group as AlOOH with symmetric hydrogen bonds (*Pnnm*), thus rationalizing the observed solid solution (Bindi et al., 2014, Am. Min.). Experiments on $MgSi(OOH)_2$ and solid solutions with AlOOH do not extend beyond 120 GPa (Nishi et al., 2014; Bindi et al., 2014, Am. Min.). The stabilization of the new orthorhombic phase of AlOOH at deep mantle conditions raises the possibility of new

stable phases in $MgSi(OOH)_2$ and on the AlOOH-$MgSi(OOH)_2$ join that may be important in super-Earth mantles or near the base of Earth's mantle.

ACKNOWLEDGEMENT

This project is supported by the European Research Council under Advanced Grant 291432 Molten Earth (FP7) to LS.

CITED REFERENCES

Alfe, D. (2009)A program to calculate phonons using the small displacement method. Computer Physics Communications, 180, 2622-2633.

Bindi, L., M. Nishi, J. Tsuchiya, T. Irifune (2014) Crystal chemistry of dense hydrous magnesium silicates: the structure of phase H, $MgSiH_2O_4$, synthesized at 45 GPa and 1000 C, American Mineralogist, 99, 1802-1805.

Blöchl, P. E. (1994)Projectors augmented-wave method. Physical Review B,50, 17953 (5).

Caracas, R. (2008) Dynamical instabilities of ice X. Physical Review Letters, 101, 085502 (4).

Cedillo, A., Torrent, M., and Cortona, P. (2016) Stability of the different AlOOH phases under pressure. Journal of Physics: Condensed Matter,28, 185401 (12).

Christensen, A. N., Gronbaek, R., and Rasmussen, S. E. (1964) The crystal structure of InOOH. Acta Chemica Scandinavica, 18, 1261-1266.

Christensen, A. N., Lehmann, M. S., Convert, P. (1985) Deuteration of crystalline Hydroxides. Hydrogen bonds of γ-AlOO(H,D) and γ-FeOO(H,D). Acta Chemica Scandinavica,**36**, 303-308.

Corbato, C. E., Tettenhorst, R. T. and Christoph, G. G. (1985) Structure refinement of deuterated boehmite. Clays and Clay Minerals,33, 71-75.

Duan, Y., Sun, N., Wang, S., Li, X., Guo, X., Ni, H., Prakapenka, V. B., Mao, Z. (2018) Phase stability and thermal equation of state of δ-AlOOH: Implication for water transportation to the Deep Lower Mantle. Earth and Planetary Science Letters, 494, 92.

Friedrich, A., Wilson, D. J., Haussuhl, E., Winkler, B., Morgenroth, W., Refson, K., and Milman, V. (2007)High-pressure properties of diaspore, AlO(OH).Physics and Chemistry of Minerals, 34, 145-157.

Furukawa, A. S. , Komatsu, K., Vanpeteghem, C. B. , and Ohtani, E. (2008) Neutron diffraction study of δ-AlOOD at high pressure and its implication for symmetrization of the hydrogen bond. American Mineralogist, 93, 1558-1567.

Goncharov,A. F., Struzhkin, V.V., Somayazulu,M. S., Hemley,R. J., and Mao,H. K. (1996)Compression of ice to 210 gigapascals: Infrared evidence for a symmetric hydrogen-bonded phase. Science, 273, 218-220.

Hill, R . J. (1979) Crystal structure refinement and electron density distribution in diaspore. Physics and Chemistry of Minerals, 5, 179-200.

Karki, B. B., Warren, M. C., Stixrude, L. , Auckland, G. J., and Crain, J. (1997) Ab initio studies of high-pressure structural transformations in silica. Physical Review B,55, 3465-3472.

Kechin, V. V. (2001) Melting curve equations at high pressure, Physical Review B, 65, 052102.

Kimura, T., Kuwayama, Y., and Yagi, T. (2011)Melting temperatures of H_2O up to 72 GPa measured in a diamond anvil cell using CO_2 laser heating technique. The Journal Of Chemical Physics, 140, 074501(5).

Kresse, G. and Hafner, J. (1994)Norm-conserving and ultrasoft pseudopotentials for first-row and transition elements. Journal of Physics: Condensed Matter, 6, 8245 – 8257.

Kresse, G. and Furthmuller, J. (1996)Efficiency of ab-initio total energy calculations for metals and semiconductors using a plane-wave basis set. Computational Material Science,6, 15-50.

Kresse, G. and Joubert, D. (1999) From ultrasoft pseudopotentials to the projector augmented-wave method. Physical Review B, 59, 1758-1775.

Kuribayashi, T., Furukawa, A. S., and Nagase, T. (2014) Observation of pressure-

induced phase transition of δ-AlOOH by using single-crystal synchrotron X-ray diffraction method. Physics and Chemistry of Minerals, 41, 303-312.

Li, S., Ahuja, R., and Johansson, B. (2006) The elastic and optical properties of the high-pressure hydrous phase δ-AlOOH. Solid State Communications, 137, 101-106.

Lyakhov, A. O., Oganov, A. R., Stokes, H. T. and Zhu, Q. (2013)New developments in evolutionary structure prediction algorithm USPEX. Computer Physics Communications, 184, 1172-1182.

Mao, H. K., Shu, J., and Hemley, R. J. (1994) High pressure X-ray diffraction study of diapsore. Solid State Communication, 90, 497-500.

Martonák, R., Donadio, D., Oganov, A. R., and Parrinello, M. (2006)Crystal structure transformations in SiO_2 from classical and ab initio metadynamics. Nature Materials, 5, 623- 626.

Millot, M., S. Hamel, J. R. Rygg, P. M. Celliers, G. W. Collins, F. Coppari, D. E. Fratanduono, R. Jeanloz, D. C. Swift, and J. H. Eggert (2018) Nature Physics, 14, 297-302.

Modak, P. and Verma, A. K. (2011) First-principles investigation of electronic, vibrational, elastic, and structural properties of ThN and UN up to 100 GPa. Physical Review B, 84, 024108 (9).

Modak, P. and Verma, A. K. (2017)Prediction of a novel 10-fold gold coordinated structure in $AuIn_2$ above 10 GPa. Physical Chemistry Chemical Physics, 19, 3532-3537.

Momma, K. and Izumi, F. (2008) VESTA: a three-dimensional visualization system for electronic and structural analysis.Journal of Applied Crystallography,41, 653-658.

Monkhorst, H. J. and Pack, J. D. (1976) Special points for Brillouin-zone integrations. Physical Review B,13, 5188-5192.

Neuhaus, A. (1964) Synthese strukturverhalten + valenzzustande der anorganischen materie im bereich hoher + hochster drucke, Chimia (Aarua), 18, 93.

Nikolae, N. A., Lityagina, L. M., Dyuzheva, T. I., Kulikova, L. F., and Bendeliani, N. A. (2008) Synthesis and single crystal growth of the new high-pressure phase of GaOOH. Journal of Alloys Compounds, 459, 95-97.

Nishi, M., Irifune, T., Tsuchiya, J., Tange, Y., Nishihara, Y., Fujino, K., and Higo, Y. (2014) Stability of hydrous silicate at high pressures and water transport to the deep lower mantle, Nature Geosciences, 7, 224-227.

Noel, Y., Demichelis, R., Pascale, F., Ugliengo, P., Orlando, R., and Dovesi, R. (2009) Ab initio quantum mechanical study of γ-AlOOH boehmite: Structure and vibrational spectrum, Physics and Chemistry of Minerals, 36, 47-59.

Oganov, A. R. and Glass, C. W. (2006) Crystal structure prediction using ab initio evolutionary techniques: principles and applications. The Journal of Chemical Physics, 124,244704 (15).

Oganov, A. R. Lyakhov, A. O., and Valle, M. (2011) How evolutionary crystal structure prediction works-and why. Accounts of Chemical Research, 44(3), 227-237.

Oganov, A. R. and Ono, S. (2004)Theoretical and experimental evidence for a post-perovskite phase of $MgSiO_3$ in Earth's D″ layer, Nature,430, 445-448.

Ohtani, E., Litasov, K., Suzuki, A., and Kodno, T. (2001)Stability field of new hydrous phase, δ-AlOOH, with implications for water transport into the deep mantle. Geophysical Research Letters, 28(20), 3991-3993.

Panero, W. R. and Stixrude, L. P. (2004)Hydrogen incorporation in stishovite at high pressure and symmetric hydrogen bonding in δ-AlOOH. Earth and Planetary Science

Letters, 221, 421.

Patel, N. N., Verma, A. K., Mishra, A. K., Sunder, M., and Sharma, S. M. (2017) Synthesis of unconventional stoichiometric compounds in the K-Br system at high pressures. Physical Chemistry Chemical Physics, 19, 7996-8007.

Perdew, J. P., Burke, K., and Ernzerhof, M. (1996)Generalized gradient approximation made simple. Physical Review Letters,77, 3865-3869.

Perdew, J. P. and Zunger, A.(1982) Self-interaction correction to density-functional approximations for many-electron systems. Physical Review B, 23, 5048-5079.

Sakai,T., Dekura, H., and Hirao, N. (2016) Experimental and theoretical thermal equations of state of $MgSiO_3$ post-perovskite at multi-megabar pressures. Scientific Reports **6**, 22652 (8).

Sano, A., Ohtani, E., Kondo, T., Hirao, N., Sakai, T., Sata, N., Ohisi, Y., Kikegawa, T. (2008a) Aluminous hydrous mineral δ-AlOOH as a carrier of hydrogen into the core-mantle boundary. Geophysical Research Letters, 35, L03303, 1-5.

Sano, A., Yagi, T., Okada, T., Gotou, H., Ohtani, E., Tsuchiya, J., and Kikegawa, T. (2008b) X-ray diffraction study of high pressure transition in InOOH. Journal of Mineralogical and PetrologicalSciences,103, 152-155.

Sikka, S. K. and Sharma, S. M. (2008)The hydrogen bond under pressure. Phase Transitions, 81, 907-934.

Stixrude, Lars (2014) Melting in the super-earths. Philosophical Transactions of the Royal Society A, 372, 1-13.

Stixrude,L. and Lithgow-Bertelloni,C. (2011)Thermodynamics of mantle minerals-II. phase equilibria. GeophysicalJournal International,184, 1180-1213.

Suzuki,A., Ohtani,E., and Kamada,T. (2000) A new hydrous phase δ-AlOOH synthesized at 21 GPa and 1000 °C. Physics and Chemistry of Minerals, 27, 689-693.

Teter,D. M., Hemley,R. J., Kresse,G., and Hafner,J. (1998)High pressure polymorphism in silica. Physical Review Letters,80, 2145-2148.

Tikoo, S. M. and L. T. Elkins-Tanton (2017) The fate of water within Earth and super-Earths and implications for plate tectonics, Philosophical Transations of the Royal Society A, 375, 20150394.

Tsuchiya, J., Tsuchiya, T., Tsuneyuki, S., and Yamanaka, T. (2002) First principles calculation of a high-pressure hydrous phase, δ-AlOOH. Geophysical Research Letters, 29, No. 19,1909 (15).

Tsuchiya, J., Tsuchiya, T., and Tsuneyuki, S. (2005)First-principles study of hydrogen bond symmetrization of phase D under high pressure. American Mineralogist, 90, 44-49.

Tsuchiya, J., Tsuchiya, T., and Wentzcovitch, R. M. (2008a) Vibrational properties of δ-AlOOH under pressure. American Mineralogist, 93, 477-482.

Tsuchiya, J., Tsuchiya, T., Sano, A., and Ohtani, E., (2008b) First principles prediction of new high-pressure phase of InOOH. Journal of Mineralogical and Petrological Sciences, 103, 116-120.

Tsuchiya, J., and Tsuchiya, T. (2011) First-principles prediction of a high-pressure hydrous phase of AlOOH. Physical Review B, 83, 054115 (5).

Tunega, D., Pašalić, H., Gerzabek, M. H., and Lischka, H. (2011) Theoretical study of structural, mechanical and spectroscopic properties of boehmite (γ-AlOOH)Journal of Physics: Condensed Matter,23, 404201 (10 pages).

Umemoto, K. and Wentzcovitch, R . M. (2008) Prediction of an U_2S_3-type polymorph of Al_2O_3at 3.7 Mbar. Proceedings of the National Academy of Sciences of the USA, 105, 6526-6530.

Vanpeteghem, C. B., Ohtani, E., and Kondo, T. (2002) Equation of state of the hydrous

phase δ-AlOOH at room temperature up to 22.5 GPa. Geophysical Research Letters,29 (7), 1119 (23).

Verma, A. K., Modak, P., and Sharma, S. M. (2017) Structural phase transitions in Li_2S, Na_2S and K_2S under compression. Journal of Alloys Compounds, 710, 460-467.

Walter, M. J., A. R. Thomson, W. Wang, O. T. Lord, J. Ross, S. C. McMahon, M. A. Baron, E. Melekhova, A. K. Kleppe, and S. C. Kohn (2015) The stability of hydrous silicates in Earth's lower mantle: experimental constraints from the systems $MgO\text{-}SiO_2\text{-}H_2O$ and $MgO\text{-}Al_2O_3\text{-}SiO_2\text{-}H_2O$, Chemical Geology, 418, 16-29.

Williams, Q. and Hemley, R. J. (2001) Hydrogen in the deep. Earth Annual Review of the Earth and Planetary Sciences, 29, 365-418 .

Yusa, H., Tsuchiya, T., Tsuchiya, J., Sata, N., and Ohisia, Y. (2008) α-Gd2S3-type structure in In2O3: Experiments and theoretical confirmation of a high-pressure polymorph in sesquioxide. Physical Review B,78, 092107 (4).

Zhong, X., Hermann, A., Wang, Y., and Ma, Y. (2016) Monoclinic high-pressure polymorph of AlOOH predicted from first principles. Physical Review B,94, 224110 (8).

Zhou, X., Jhang, J., Ma, Y., Tian, H., Wang, Y., Li, Y., Jiang, L., and Cui, Q. (2017) The solvothermal synthesis of γ-AlOOH nanoflakes and their compression behaviors under high pressures RSC Advances, 7, 4904-4911.

Figure 1: Static enthalpies of different structures of AlOOH relative to *Pnnm* (upper panel) and $Pa\bar{3}$ (lower panel) phases. All enthalpies are given per formula units of AlOOH. Al_2O_3+ ice enthalpy data is taken from Ref. (Zhong et al. 2016).

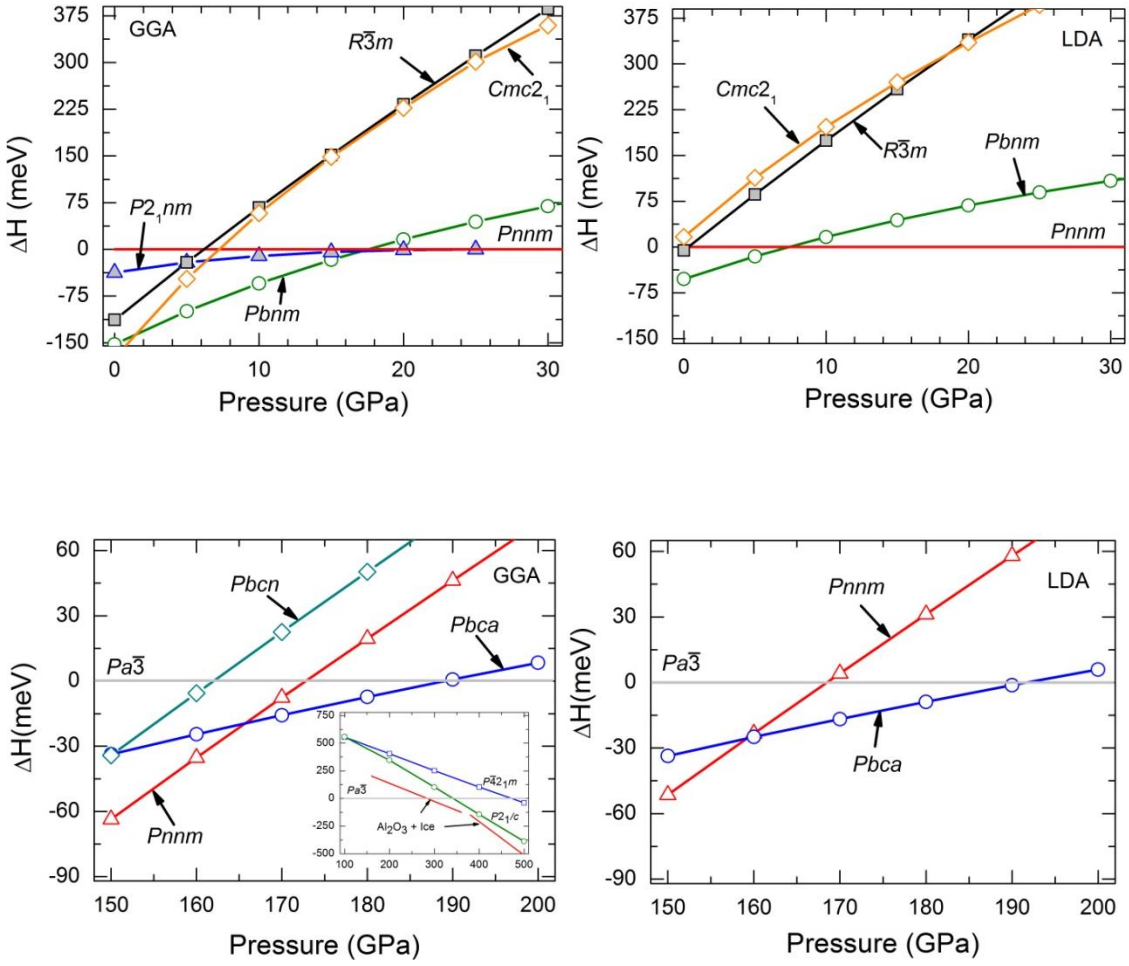

Figure2: Crystal structures of AlOOH and InOOH. Here red, faroese and orange colour balls represent hydrogen, oxygen and metal atoms, respectively. Al and O atoms that participate in edge-sharing arrangement of polyhedra are connected by grey rods (right panel). In atoms that participate in edge- and face-sharing arrangement of polyhedra are connected by grey rods (middle picture).In and O atoms in face-sharing arrangement of polyhedra are shown connected by grey rods (right picture). These figures are rendered using VESTA software (Momma and Izumi 2008).

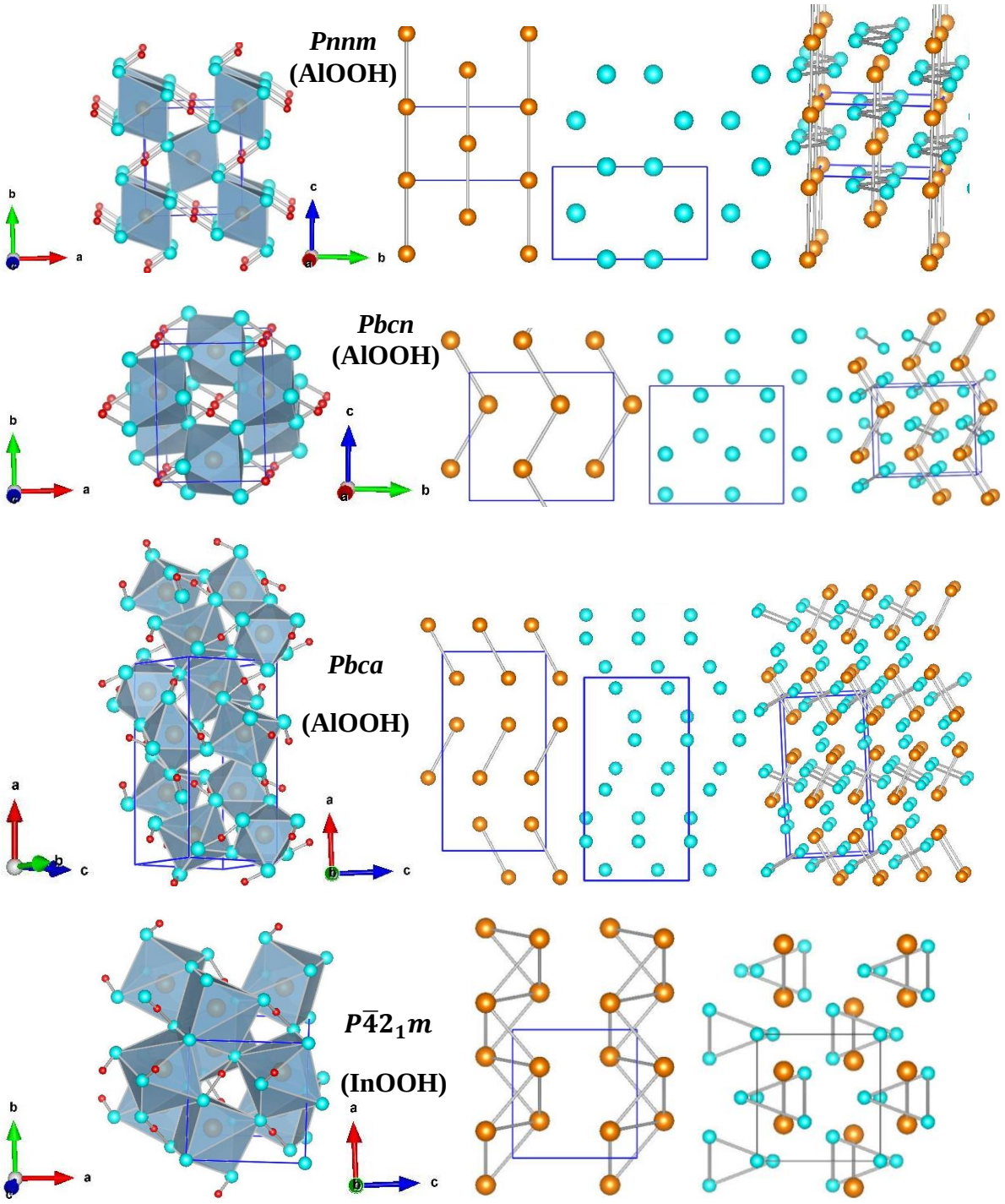

Figure 3: Relationship between R_{OO} and R_{OH} for different phases of AlOOH along with $P\bar{4}2_1m$ phase of InOOH.

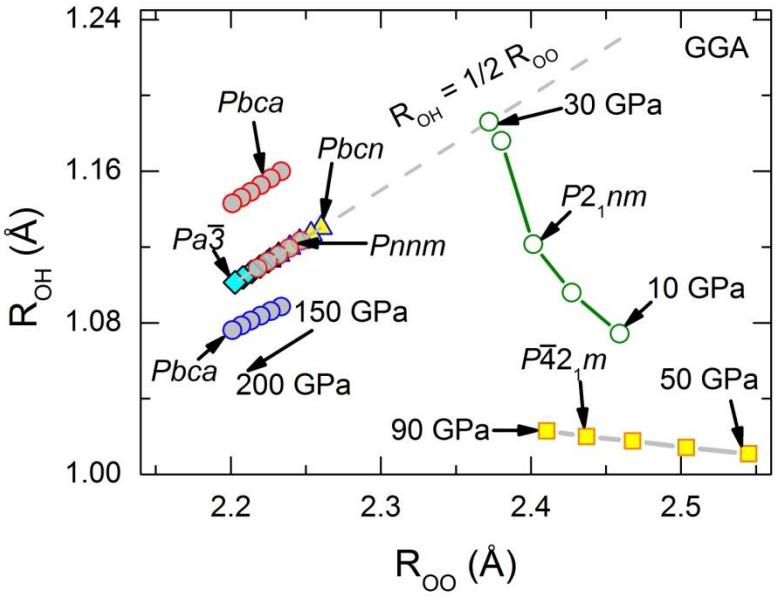

Figure 4: Pressure variation of lattice parameters of α-AlOOH (*Pbnm*, *Z* = 4) (upper panel) and *Pbca*-type AlOOH (lower panel). Filled symbols represent the experimental data (Mao et al. 1994).

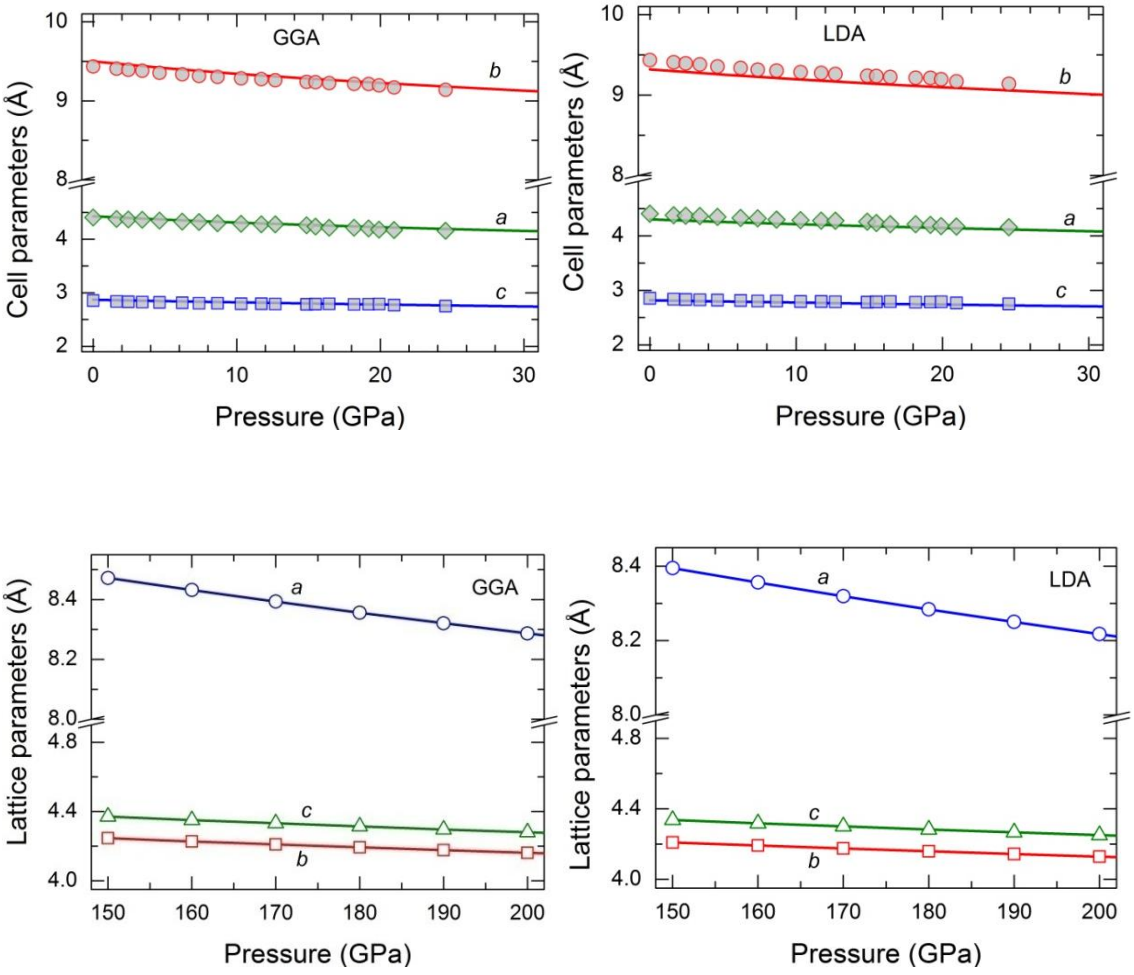

Figure 5: Pressure-volume equation-of-states of different structures in low-pressure region (upper panel). Lower panel shows the equation-of-states data of *Pnnm*, *Pbca* and $Pa\bar{3}$ structures in high-pressure region. Here volumes are given per formula unit of AlOOH. Filled triangles and diamonds represent the experimental data of α- and δ-AlOOH phases, respectively (Mao el al. 1994; Vanpeteghem et al. 2002). Filled inverted triangles show boehmite experimental data (Zhou et al. 2017).Curved arrows indicate volume drop on transition.

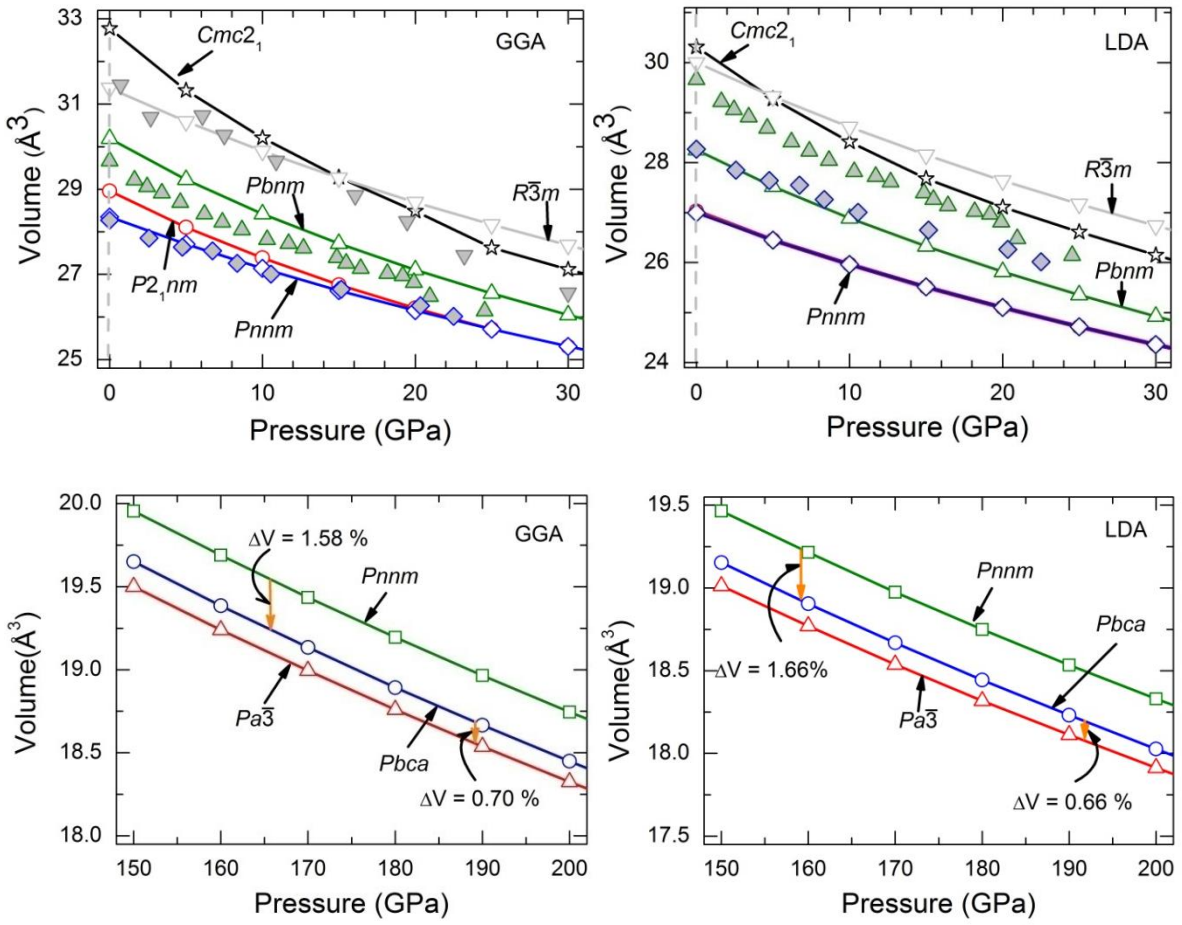

Figure 6: GGA phonon dispersion (left) and density of states (right) of *Pbca*-type AlOOH at 180 GPa.

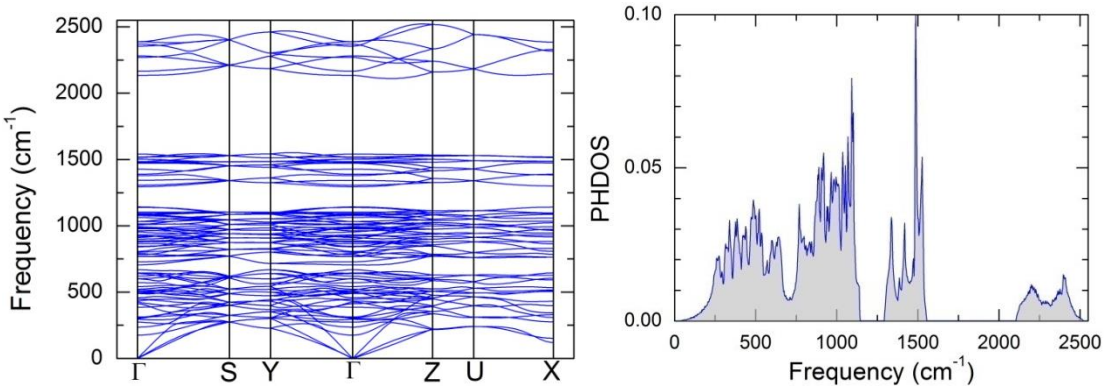

Figure 7: Phase diagram of AlOOH, showing phase boundaries among the stable crystalline structures found in our study and the decomposition to oxides from previous study (Zhong et al. 2016) (thin black lines). Also shown for comparison is the high temperature stability limit of AlOOH: bold solid black line over the range of experimental measurement (Sano et al. 2008a) and our estimated extrapolation (bold dashed black line) (Eq. 4); and the experimental dehydration boundary in the MgO-Al_2O_3-SiO_2-H_2O system (Walter et al., 2015) (thin dashed black line). We also indicate a range of probable temperature distributions in rocky planets, corresponding to the mean temperature profile (Stixrude 2014) (upper curve: 1500 K adiabat) and the temperature profile in cool, downwelling regions (lower curve: 1000 K adiabat). Adiabats are from Ref. (Stixrude and Lithgow-Bertelloni 2011).

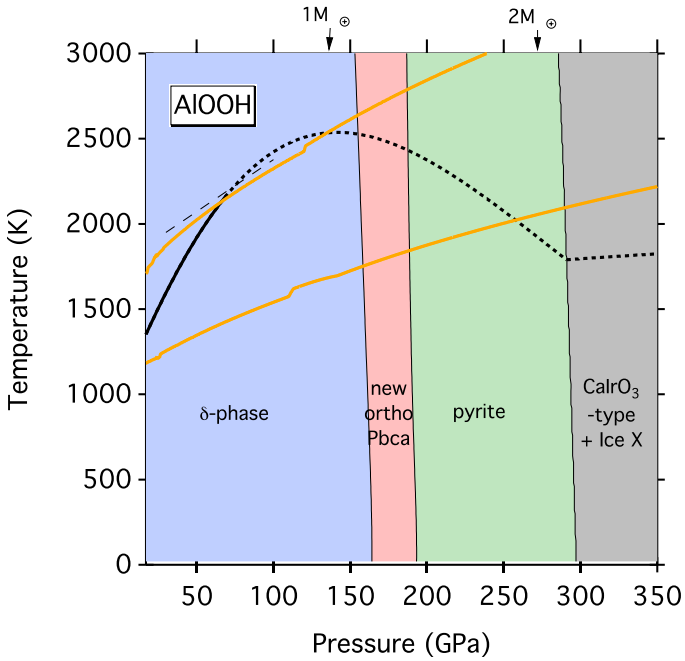

Figure 8: Static enthalpies of different structures of GaOOH relative to *Pnnm* (upper panel) and $Pa\bar{3}$ (lower panel) structures. In LDA structural optimization, $P2_1nm$ structure relaxes to *Pnnm* between 5-10 GPa. All enthalpies are given per formula units of GaOOH.

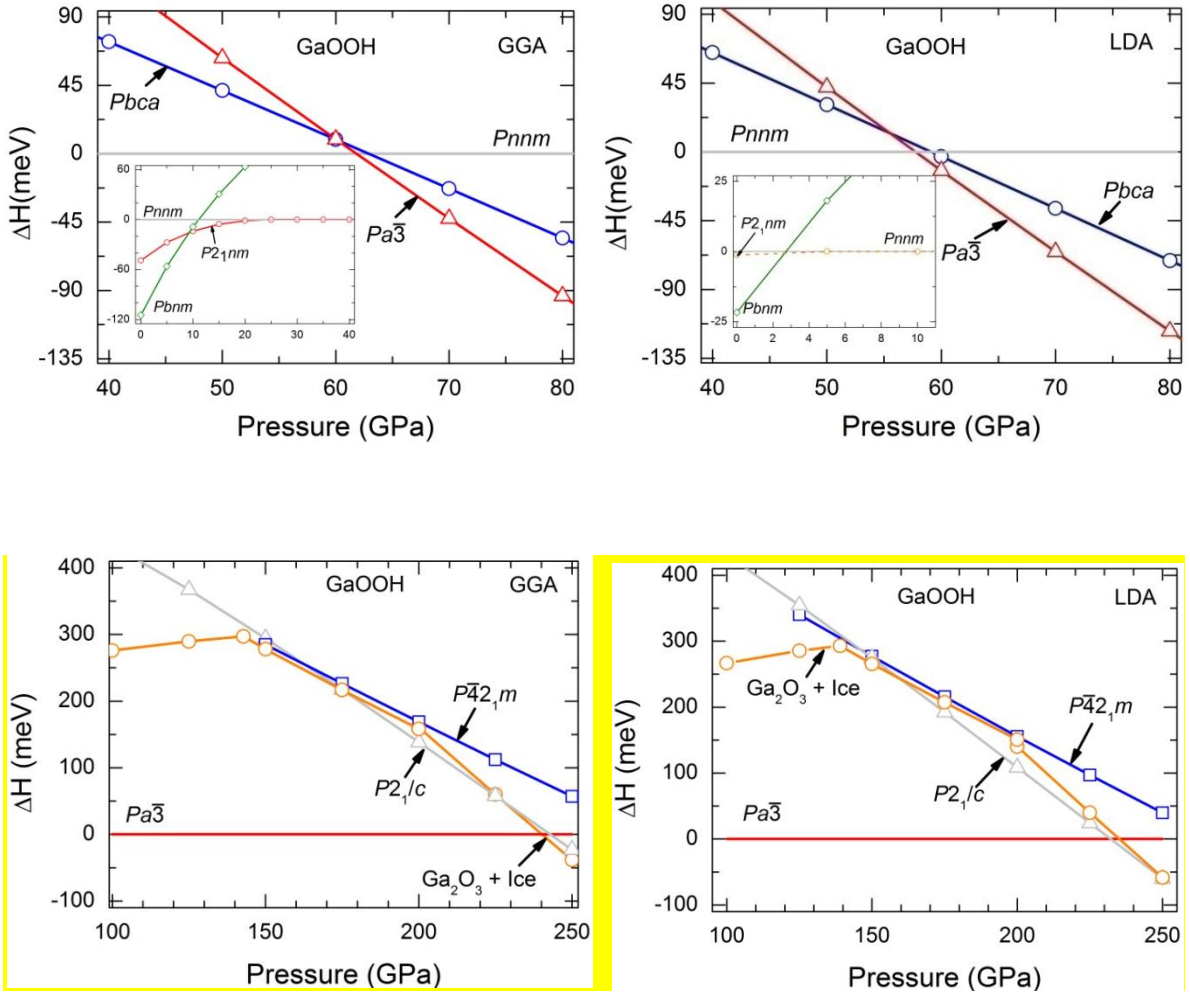

Figure 9: Static enthalpies of different structures of Ga_2O_3 relative to Rh_2O_3-II. All enthalpies are given per formula units of Ga_2O_3.

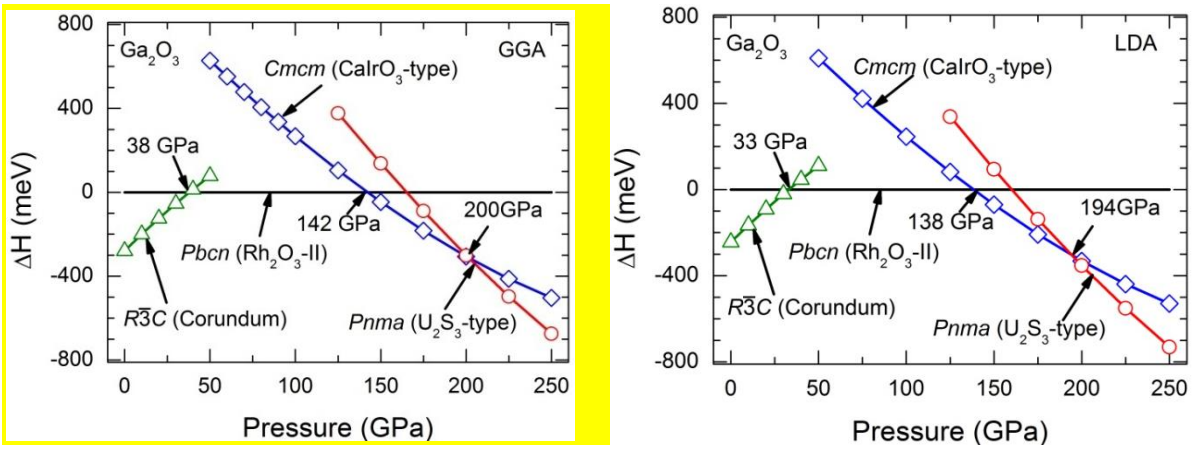

Figure 10: Static enthalpies of different structures of InOOH relative to *Pnnm* (upper panel) and $Pa\bar{3}$ (lower panel) phases. In LDA structural optimization, $P2_1nm$ structure relaxes to *Pnnm* between 0-5 GPa. All enthalpies are given per formula units of InOOH.

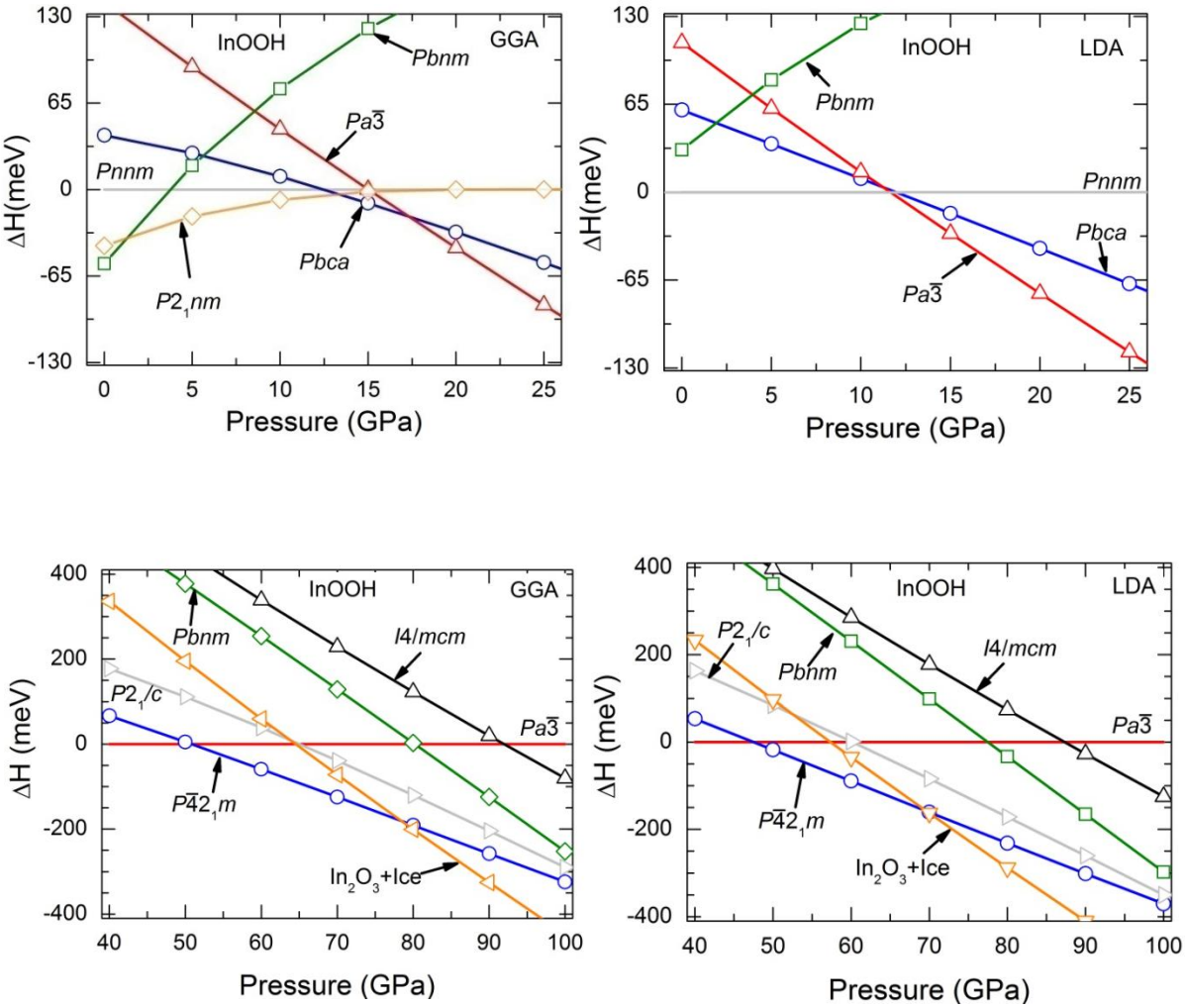

Figure 11: Lattice parameters (upper panel) and equation-of-states (lower panel) of $Pa\bar{3}$and $P\bar{4}2_1m$ phases in relevant pressure region. Here volumes are given per formula unit of InOOH.

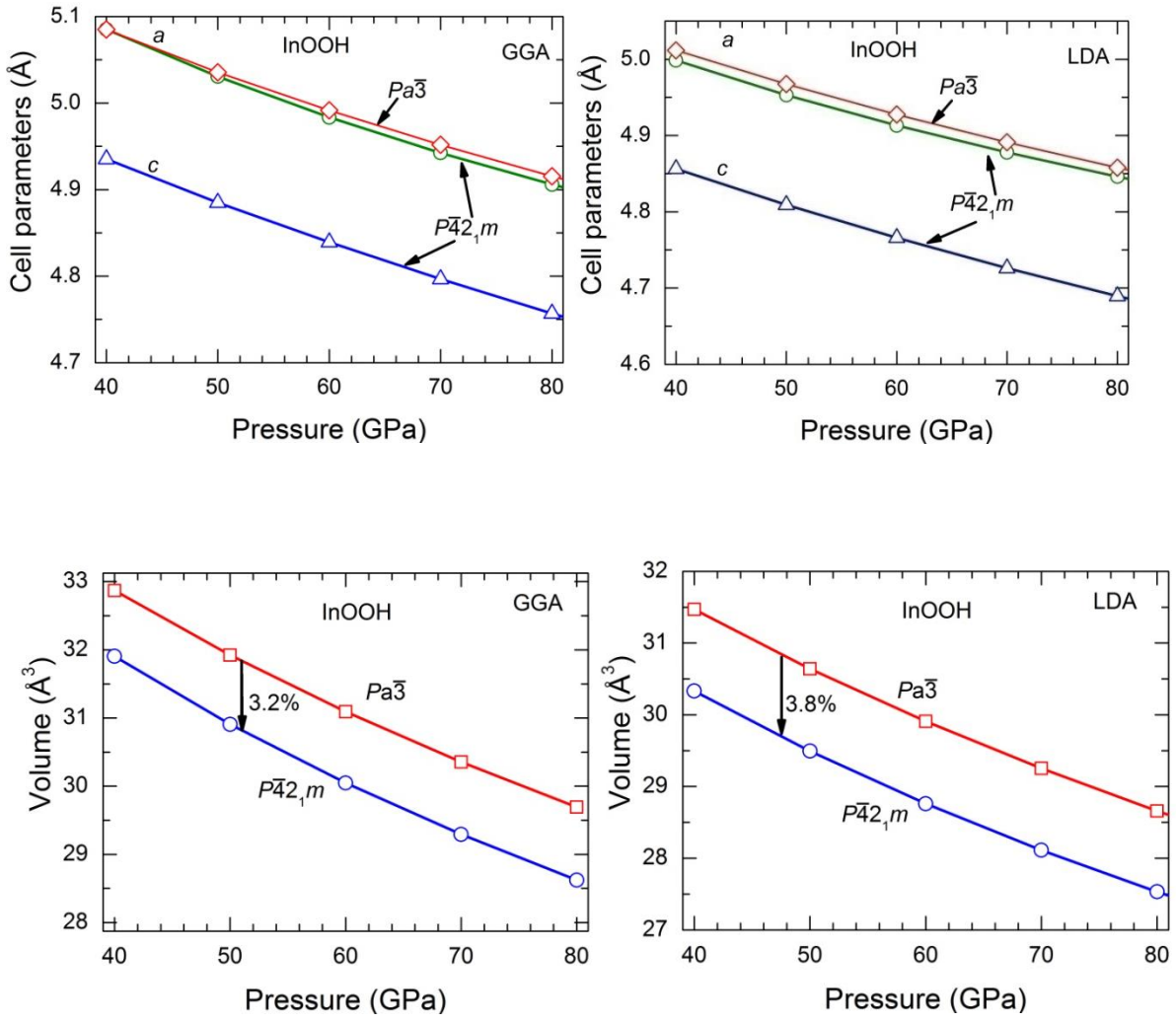

Figure 12: GGA phonon dispersion (left) and density of states (right) of $P\bar{4}2_1m$ type InOOH at 60 GPa.

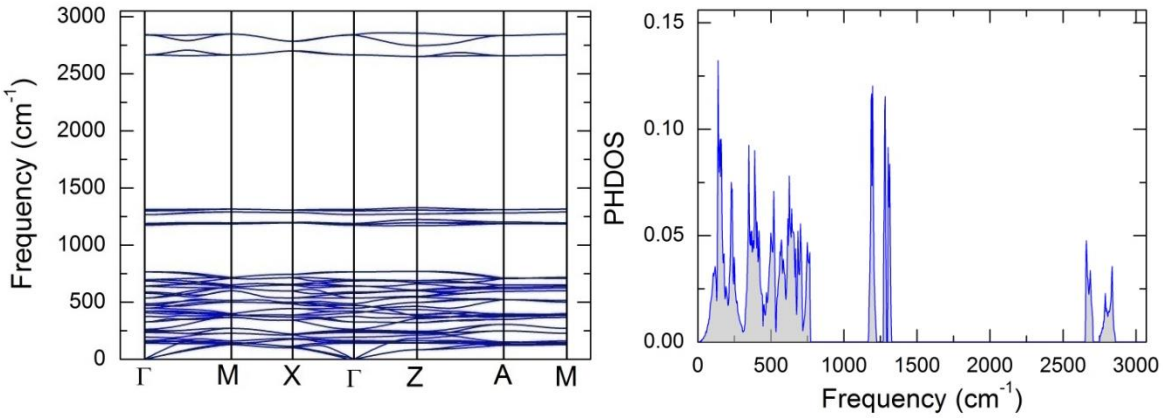

Table I: Pressure at which each phase first becomes stable in the three systems considered according to our GGA calculations. Dashes indicate that the phase has no stability field at static conditions. Italics indicates the phase is everywhere less stable than the component oxides: $M_2O_3+H_2O$ (M=Al, Ga, In). Experimental values (where available) in parentheses. The change in symmetry upon H-bond symmetrisation is indicated for the δ phase.

Name	SG	SG no.	Z	AlOOH	GaOOH	InOOH
δ	$P2_1nm \rightarrow Pnnm$	31→58	2→2	17.1(17)[a]	9.3(8.5)[b]	1.3(0)[c]
New orthorhombic phase	$Pbca$	61	8	165.7	-	12.4
Pyrite	$Pa\bar{3}$	205	4	189.1	61.8	17.3(14)[d]
Monoclinic	$P2_1/c$	14	4	*341.4*	*243.0*	-
New tetragonal phase	$P\bar{4}2_1m$	113	4	-	-	50.8

[a]Ohtani et al. (2001)

[b]Nikolae et al. (2008)

[c]Christensen et al. (1964)

[d]Sano et al. (2008b)

Table II: Crystallographic data of newly proposed structures as obtained in GGA calculations.

	P (GPa)	Lattice parameters (Å)	Atomic coordinates
AlOOH *Pbca*	180	*a* = 8.3561 *b*= 4.1928 *c*= 4.3139	Al (8*c*):0.63350 0.50710 0.13820 O1 (8*c*):0.19200 0.34960 0.01710 O2 (8*c*):0.55240 0.84190 0.29950 H (8*c*):0.89390 0.50350 0.13410
InOOH *Pbca*	15	*a* = 10.5183 *b*= 5.2393 *c*= 5.3459	In (8*c*): 0.63429 0.49934 0.66606 O1 (8*c*): 0.18625 0.36943 0.47282 O2 (8*c*): 0.56047 0.86024 0.80563 H (8*c*): 0.89058 0.48489 0.67787
InOOH $P\bar{4}2_1m$	60	*a* = 4.9853 *b*= 4.9853 *c*= 4.8393	In (4*e*): 0.29049 0.79049 0.21637 O1 (4*e*): 0.19138 0.69138 0.61417 O2 (2*a*): 0.00000 0.00000 0.00000 O2 (2*c*): 0.00000 0.50000 0.12969 H (4*e*):0.31513 0.81513 0.72119
Ga_2O_3 **(U_2S_3-type)** *Pnma*	225	*a* = 6.9377 *b*= 2.5088 *c*= 6.9593	Ga1 (4*c*): 0.98374 0.25000 0.30999 Ga2 (4*c*): 0.30584 0.25000 0.40922 O1 (4*c*): 0.22293 0.25000 0.20001 O2 (4*c*): 0.05281 0.25000 0.87553 O3 (4*c*): 0.38300 0.25000 0.94202